

Synthesis, Photophysical, Electrochemical, Tumor-Imaging, and Phototherapeutic Properties of Purpurinimide-N-substituted Cyanine Dyes Joined with Variable Lengths of Linkers

Michael P. A. Williams,[†] Manivannan Ethirajan,[†] Kei Ohkubo,[§] Ping Chen,^{||} Paula Pera,[†] Janet Morgan,[‡] William H. White, III,[†] Masayuki Shibata,^{*,†} Shunichi Fukuzumi,^{*,§,#} Karl M. Kadish,^{*,||} and Ravindra K. Pandey^{*,†}

[†]PDT Center, Department of Cell Stress Biology, Roswell Park Cancer Institute, Buffalo New York 14263, United States

[‡]Department of Dermatology, Roswell Park Cancer Institute, Buffalo New York 14263, United States

[§]Department of Material and Life Sciences, Graduate School of Engineering, Osaka University, ALCA, Japan Science and Technology Agency (JST), Osaka, Japan

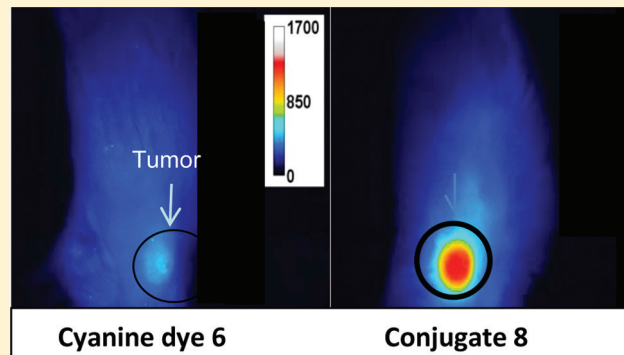
^{||}Department of Chemistry, University of Houston, Houston, Texas 77204-5003, United States

[†]Department of Health Informatics, University of Medicine & Dentistry of New Jersey—SHRP, Newark, New Jersey 07107, United States

^{*}Department of Bioinspired Science, Ewha Womans University, Seoul 120-750, Korea

Supporting Information

ABSTRACT: Purpurinimide methyl esters, bearing variable lengths of N-substitutions, were conjugated individually to a cyanine dye with a carboxylic acid functionality. The results obtained from *in vitro* and *in vivo* studies showed a significant impact of the linkers joining the phototherapeutic and fluorescence imaging moieties. The photosensitizer–fluorophore conjugate with a PEG linker showed the highest uptake in the liver, whereas the conjugate linked with two carbon units showed excellent tumor-imaging and PDT efficacy at 24 h postinjection. Whole body imaging and biodistribution studies at variable time points portrayed enhanced fluorescent uptake of the conjugates in the tumor compared to that in the skin. Interestingly, the conjugate with the shortest linker and the one joining with two carbon units showed faster clearance from normal organs, e.g., the liver, kidney, spleen, and lung, compared to that in tumors. Both imaging and PDT efficacy of the conjugates were performed in BALB/c mice bearing Colon26 tumors. Compared to the others, the short linker conjugate showed poor tumor fluorescent properties and as a corollary does not exhibit the dual functionality of the photosensitizer–fluorophore conjugate. For this reason, it was not evaluated for *in vivo* PDT efficacy. However, in Colon26 tumor cells (*in vitro*), the short linker was highly effective. Among the conjugates with variable linkers, the rate of energy transfer from the purpurinimide moiety to the cyanine moiety increased with decreasing linker length, as examined by femtosecond laser flash photolysis measurements. No electron transfer from the purpurinimide moiety to the singlet excited state of the cyanine moiety or from the singlet excited state of the cyanine moiety to the purpurinimide moiety occurred as indicated by a comparison of transient absorption spectra with spectra of the one-electron oxidized and one-electron reduced species of the conjugate obtained by spectroelectrochemical measurements.



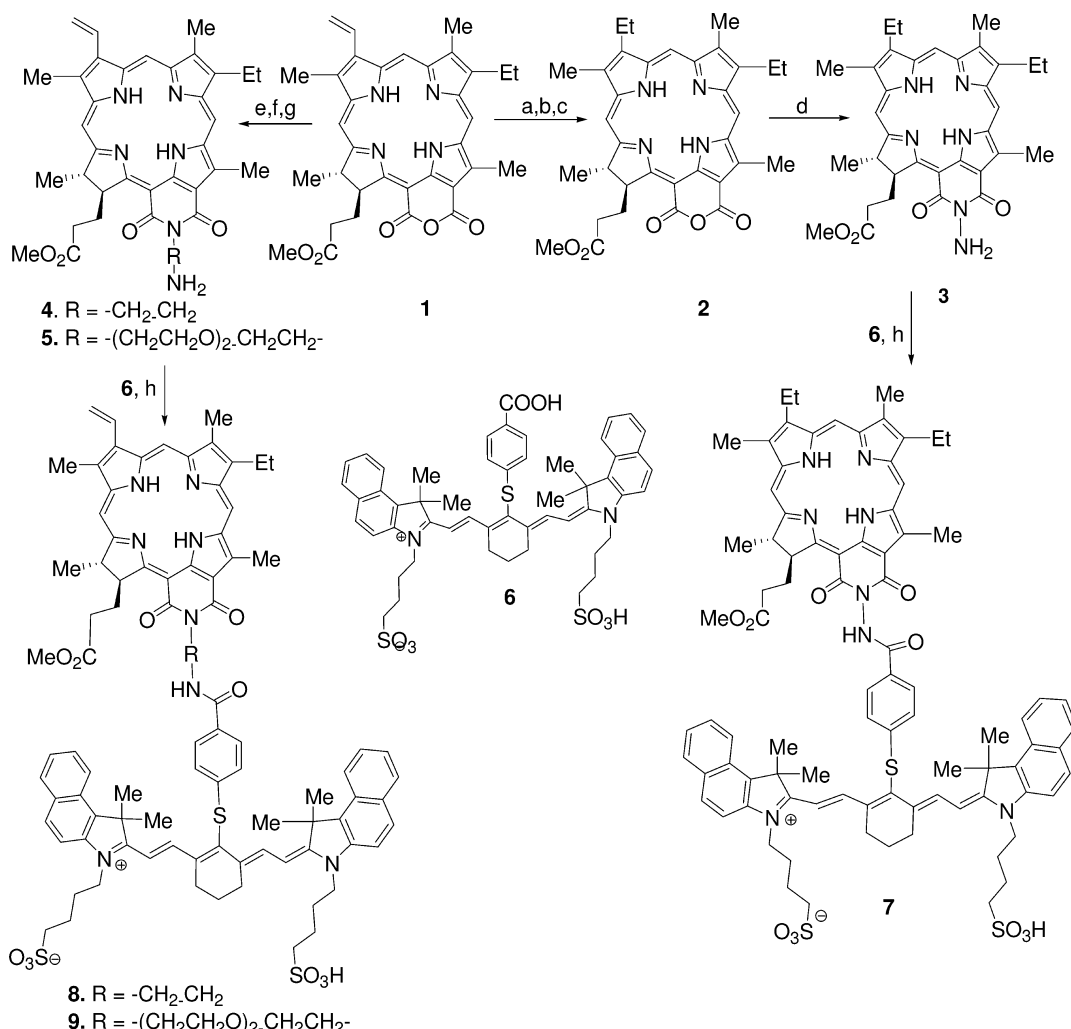
1. INTRODUCTION

Current treatment modalities for patients afflicted by cancer include surgery, radiation therapy, chemotherapy, and a relatively novel option called photodynamic therapy (PDT).^{1–5} Surgery is used to excise abnormal growths and surrounding tissue, but the procedure is invasive and may be complicated by relapse of the cancer if not all of the tumor cells are removed. Chemotherapy employs different cytotoxic chemicals to attack or block specific cellular and molecular mechanisms that aid tumor growth. Unfortunately, patients on

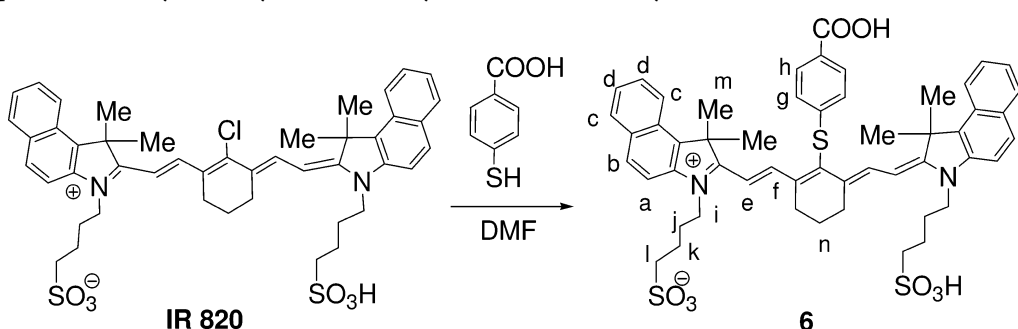
chemotherapeutics suffer from side effects due to adverse drug toxicities. Radiation uses ionizing energy to attack neoplastic cells, but it is nonspecific and may cause damage to surrounding healthy tissue, which can lead to the occurrence of secondary cancers. PDT uses a drug known as a photosensitizer, light, and oxygen to destroy tumors and their surrounding vasculature.

Received: June 30, 2011

Revised: September 14, 2011

Scheme 1. Synthesis of Purpurinimide–Cyanine Dye Conjugates Joined with Variable Lengths of Linkers^a

^aReagents and conditions: (a) Zn(OAc)₂, reflux in MeOH, 2 h; (b) Pd/carbon, H₂ THF, 12 h; (c) TFA, 2 h, RT; (d) NH₂–NH₂(anhydrous), pyridine DCM/HCl, RT; (e) R₁=(CH₂)_n, DCM, CH₂N₂, KOH/MeOH; (f) R₂=(C₂H₄O)₂C₂H₄, CH₂N₂, KOH/MeOH; (g) DCM/TFA (1:4), 2 h; (h) DMTMM, DMF, 12 h.

Scheme 2. Preparation of a Cyanine Dye with Carboxylic Acid Functionality

PDT has several advantages in that (i) there is no systemic, organ, or tissue toxicity, (ii) it is noninvasive, and (iii) it can be used repeatedly as a primary or adjuvant treatment.^{6–9} With the current advent of imaging technologies to monitor tumor responses to treatment, we have shown that the utilization of a certain photosensitizer–cyanine dye conjugate which contains the tumor-avid photosensitizer 3-(1'-hexyloxyethyl)-pyropheophorbide-a (HPPH) for treatment and a fluorophore cyanine

dye for optical imaging could be highly advantageous to treat deeply seated tumors and monitor the treatment response.¹⁰ The ability to image real time events using fluorescence has made optical imaging an attractive modality to study cellular and molecular events¹¹ and to visualize events *in vivo*, especially in tumors.¹² Noninvasive in nature, optical imaging instruments are simpler and less expensive to operate and can allow precise assessment of the location and size of a tumor, providing

information on its invasiveness in adjacent tissue.^{13,14} The work discussed herein describes the synthesis, molecular modeling, photophysical, electrochemical, tumor-imaging, and the phototherapeutic potential of a series of longer wavelength photosensitizer (purpurinimides, 700 nm) joined to a cyanine dye with variable lengths of linkers. Among the near-infrared (NIR) dyes, cyanine dyes in general have shown enormous potential for optical imaging.^{15–19}

2. RESULTS AND DISCUSSION

2.1. Chemistry. For the synthesis of purpurinimide-*N*-substituted cyanine dye conjugates, purpurin-18 methyl ester **1** was synthesized from chlorophyll-a by following the literature procedure, which was converted into mesopurpurin-18 methyl ester **2** by following the standard methodology.²⁰ Reaction of **2** with hydrazine hydrate gave N-amino mesopurpurin-18 methyl ester **3** in 50% yield.²¹ By following a similar approach, **1** was individually reacted with diethyl diamine and carbamic acid to produce the corresponding N-substituted analogues **4** and **5** both with 89% yield. Reaction of these N-substituted purpurin-18 methyl esters with a cyanine dye **6** containing a carboxylic acid functionality (obtained in 80% yield by reacting commercially available IR820 with *p*-thiol-benzoic acid) gave purpurinimide–cyanine dye conjugates **7–9** in which two chromophores (photosensitizer and fluorophore) are joined at variable linker lengths with yields ranging from 32 to 37%. The reaction sequences for the preparation of the conjugates and the cyanine dyes are shown in Schemes 1 and 2.

Structures of the intermediates and the final products were confirmed by ¹H NMR and CHN/mass spectrometry (including HRMS) analysis. The purity of the final conjugates (compounds **7–9**) was determined by HPLC analysis.

2.2. Molecular Modeling. In order to examine the effects of linker lengths joining the two chromophores (conjugates **7**, **8**, and **9**) in photophysical, electrochemical, tumor-imaging and photodynamic efficacy, a molecular modeling study was performed. The three-dimensional model of the conjugates were built with the molecular modeling software SYBYL (Tripos Inc., St. Louis, MO) followed by the energy minimization with the PM3 semiempirical molecular orbital theory using the Spartan 02 software package (Wave function Inc., Irvine, CA). Figure 1 shows the resulting structures of the

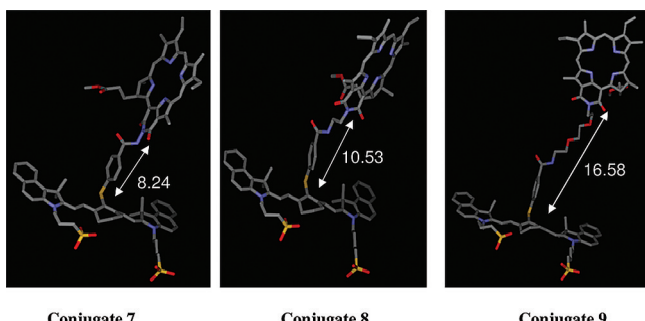


Figure 1. Three-dimensional representation of the conjugates with different lengths between the cyanine dye and the purpurinimide in extended conformation obtained from molecular modeling and energy optimization with PM3.

conjugates **7**, **8**, and **9** (Scheme 1) in extended conformation. The distances between the nitrogen atom in the purpurinimide ring system and the sulfur atom adjacent to the cyanine dye of

the conjugates were calculated and are displayed in Figure 1. As expected, the smaller the linker length, the shorter the observed distance between two chromophores.

Since the above structures are appropriate for single molecules in gas phase, they may not be relevant to the structures of the conjugates in solution, in cells, or *in vivo* environments where physical properties and biological activities of these conjugates are examined. In order to gain some insights, the conformational flexibility of these conjugates were examined with the stochastic search module of MOE software using the MMFFs force field and charges (Chemical Computing Group, Montreal, Quebec, Canada). Again, the distance between two chromophores was measured for some of the resulting low energy conformers as shown in Figure 2.

As can be seen from the Figure 2 caption, the distances between the two chromophores remain more or less constant for conjugates **7** and **8**, while it shows a large variation for conjugate **9**. It is reasonable considering the length of the linker for these conjugates. Although the mean distances are similar between conjugates **7** and **8**, closer inspections reveal the significant difference between these conjugates. First, the standard deviation is much smaller for conjugate **7** than for **8**, reflecting the limited flexibility of **7**. Second, this limited flexibility is also the source of the limited range in the relative orientation of two chromophores for conjugate **7** as shown in Figure 2a where various low energy conformers of conjugate **7** are superimposed using the purpurinimide ring as a reference. It clearly shows that the cyanine dye and the linker can assume many different conformations but that they cannot assume a conformation that brings two chromophores close together. Thus, the purpurinimide ring remains exposed to its surroundings for this conjugate. Compared to conjugate **7**, some part of the purpurinimide ring is covered by the cyanine dye or thiophenol group in conjugate **8**, as shown in Figure 2b. Although there are a large variety of conformers for conjugate **9**, there are some conformers where a large portion of the purpurinimide ring is covered by the cyanine dye and/or thiophenol group as shown in Figure 2c. Photophysical experiments clearly indicated that intramolecular energy transfer occurred from the singlet excited state of the purpurinimide moiety to the cyanine moiety with the rate of transfer increasing with decreasing linker distance. This is an opposite trend from the linker length dependence on the *in vitro* PDT efficacy. The photophysical results are consistent with the distance dependence of energy transfer, while the conformational flexibility may explain the excellent *in vitro* PDT efficacy of conjugate **7** and the decrease of efficacy with increasing linker length. If the purpurinimide rings are not exposed to the environment, the compound may not be able to produce singlet oxygen because it cannot interact with water molecules. Alternatively, even if singlet oxygen is produced, it may not reach to the cellular target because the singlet oxygen produced may interact with the closely seated cyanine dye before it reaches the target site(s).

2.3. Photodynamics. In order to examine the photodynamics of purpurinimide, cyanine, and the conjugates, time-resolved transient absorption spectra were recorded by femtosecond laser flash photolysis in deaerated DMSO solutions as shown in Figure 3. Transient absorption bands of purpurinimide **4** observed at 500 and 530 nm taken at 2 ps after femtosecond laser excitation (Figure 3a) are assigned as the singlet excited state of **4** (¹4*). The transient absorption of ¹4* decreased as the absorption band of the triplet excited state

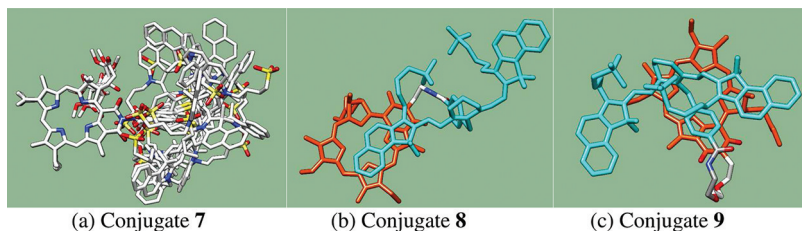


Figure 2. (a) Various conformers for conjugate 7 with limited flexibility in the linker are superimposed using the purpurinimide ring as reference. Standard color for each atom type is used. The purpurinimide ring (shown in the left portion of this figure) is exposed to surroundings. (b) Examples of the low energy conformer for conjugate 8. The purpurinimide moiety is shown in orange and the cyanine dye–thiophenol moiety in cyan, and the linker regions are based on standard atom type based color. There are some overlaps between the purpurinimide ring and the cyanine dye ring. (c) Example of the low energy conformer for conjugate 9. The same color scheme as that in panel b is used. Because of the flexibility of the long linker, diverse conformations are possible, and some of the low energy conformers show an extensive interaction between the purpurinimide ring and the cyanine dye–thiophenol moiety. Mean distance between the two moieties in panel a (conjugate 7) = 8.18 Å (SD 0.10); in panel b (conjugate 8) = 8.55 Å (SD 0.51); and in panel c (conjugate 9) = 9.85 Å (SD 2.27).

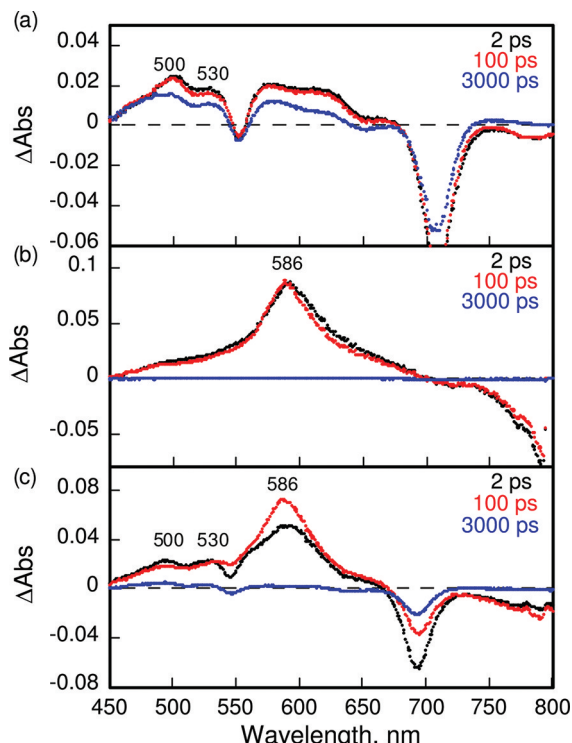


Figure 3. Transient absorption spectra of purpurinimide 4, cyanine 6, and conjugate 7 in deaerated DMSO taken at 2, 100, and 3000 ps after femtosecond laser flash excitation at 410 nm.

of 4 appeared. The transient absorption band of the singlet excited state of cyanine 6 is observed at 586 nm as shown in Figure 3b. The lifetimes of the singlet excited state of 4 and 6 were determined from decays of the absorption at >3 ns and 500 ps, respectively. In the case of conjugate 7 shown in Figure 3c, the transient absorption bands due to both singlet excited states of purpurinimide and cyanine were observed at 500, 530, and 586 nm at 2 ps because both moieties were excited by laser flash excitation at 410 nm. The absorption bands at 500 and 530 nm due to the singlet excited state of the purpurinimide moiety decreased, accompanied by an increase in the absorption band at 586 nm due to the singlet excited state of the cyanine moiety. This indicates that energy transfer from the singlet excited state of purpurinimide to the cyanine moiety occurs efficiently to afford the singlet excited state of cyanine. The energy transfer dynamics in 7 were determined from the

rise of the absorption band at 586 nm as shown in the left panel of Figure 4a. The energy transfer rate constant was determined to be $6.7 \times 10^{11} \text{ s}^{-1}$. Similarly, the energy transfer rate constants of conjugates 8 and 9 were also determined from the rise of the absorption band at 586 nm in Figure 4b and c to be 1.4×10^{11} and $1.3 \times 10^{11} \text{ s}^{-1}$, respectively. The energy transfer rate constant increases with decreasing distance between the energy donor and acceptor estimated from the theoretical calculations (*vide supra*). The decay time profiles at 586 nm are shown on the right side of Figure 4. The decay rate constants of 7–9 agree well with the value of the cyanine reference 6 due to intersystem crossing to the triplet excited state. An energy transfer from the singlet excited state of the purpurinimide moiety to the cyanine moiety is feasible because the singlet energy of the purpurinimide (1.76 eV) is higher than that of the cyanine (1.41 eV), which were obtained from the absorption and fluorescence maxima, $\lambda_{\text{abs}} = 689 \text{ nm}$ and $\lambda_{\text{fl}} = 720 \text{ nm}$ for 4, and $\lambda_{\text{abs}} = 849 \text{ nm}$ and $\lambda_{\text{fl}} = 915 \text{ nm}$ for 6, respectively. Thus, in the purpurinimide–cyanine systems, intramolecular energy transfer at the singlet excited state occurs efficiently from the purpurinimide moiety to the cyanine moiety, followed by intersystem crossing to the triplet excited state of the cyanine moiety. No electron transfer from the purpurinimide moiety to the cyanine moiety was observed as expected from the disfavored energetics as indicated by the redox potentials of the conjugates (*vide infra*).

2.4. Electrochemical Properties. Cyclic voltammograms of 7–9 are illustrated in Figure 5, which also includes the reference compounds 4 and 6. The first one-electron oxidation potentials of 7–9 (E_{ox}) are all located at $E_{1/2} = 0.52 \text{ V}$ vs SCE, which is similar to the E_{ox} value of compound 6 (0.56 V vs SCE). The first one-electron reduction potentials of 7–9 (E_{red1}) are also identical at $E_{1/2} = -0.55 \text{ V}$ vs SCE, which agrees with the E_{red1} value of cyanine 6 (-0.56 V vs SCE). The second one-electron reduction potentials of 7–9 (E_{red2}) are also nearly the same and range from -0.64 to -0.69 V vs SCE, which agree with the E_{red1} value of compound 4 (-0.69 V vs SCE). Thus, there seems to be little or no interaction between the purpurinimide and cyanine moieties in the conjugates 7–9, irrespective of the difference in the distance between them.

The second one-electron oxidation of the purpurinimide moiety of the conjugates 8 and 9 is irreversible, and the peak potential ranges from 0.89 to 0.92 V vs SCE, which is similar to that of 4 (0.94 V). The energy of the charge-separated state of 7–9 to be produced by electron transfer from the purpurinimide moiety to the singlet excited state of the cyanine

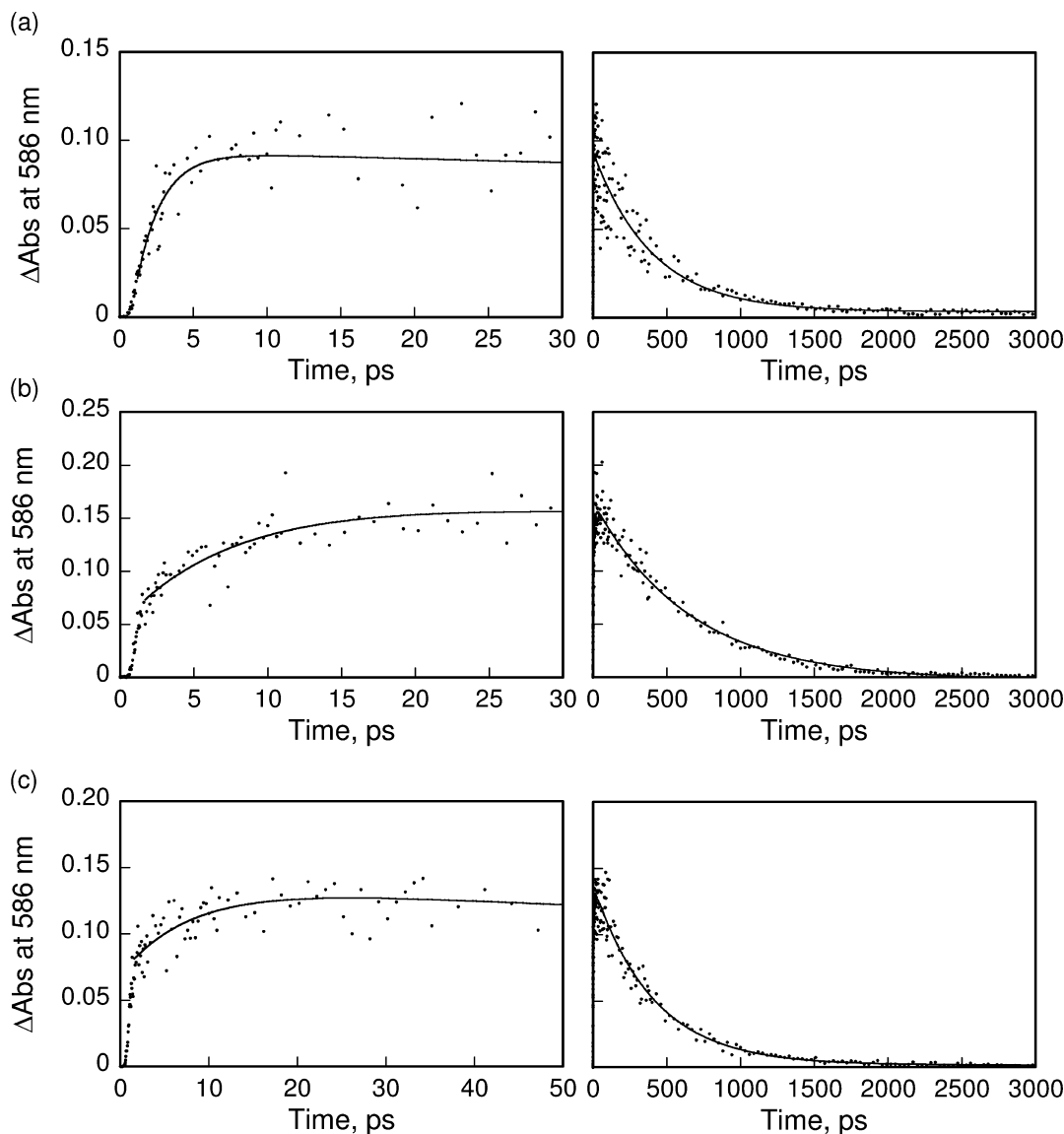


Figure 4. Rise and decay time profiles of the absorbance at 586 nm of (a) 7, (b) 8, and (c) 9 in deaerated DMSO after femtosecond laser excitation at 410 nm. Left panels: short time range. Right panels: long time range.

moiety is roughly estimated to be 1.6 eV, which is higher than the energy of the singlet excited state of cyanine (1.41 eV). The energy of the charge-separated state of **7–9** in the reverse direction from the singlet excited state of the cyanine moiety to the purpurinimide moiety is also estimated to be 1.74 eV, which is higher than the energy of the singlet excited state of cyanine (1.41 eV). Thus, electron transfer from the singlet excited state of the cyanine moiety to the purpurinimide moiety is energetically feasible. However, no electron transfer occurred from the purpurinimide moiety to the singlet excited state of the cyanine moiety as shown in Figure 3. This indicates that the intersystem crossing from the singlet excited state of the cyanine moiety to the triplet excited state is much faster than the electron transfer.

The absence of a charge-separated state of **7–9** was further confirmed by measuring the purpurinimide radical cation and the cyanine radical anion by use of a spectroelectrochemistry (*vide infra*). Figure 6a shows the spectral changes (in blue) which occurred during the one-electron reduction of cyanine **6** at an applied potential of -0.70 V. A new absorption maximum

at 531 nm, which is assigned to the cyanine radical anion, appears, and this was accompanied by a disappearance of absorption bands at 773 and 849 nm due to cyanine. A clean isosbestic point is seen in this transfer. The radical anion can be further reduced to the dianion at an applied potential of -1.60 V vs SCE. A similar spectral change is observed for the first one-electron reduction of conjugate **7** (Figure 6b), where the radial anion of the cyanine moiety has an absorption band at 533 nm. Figure 6c shows the spectral changes upon the one-electron reduction of purpurinimide **4** at an applied potential of -0.90 V, in which the Soret band at 417 nm and the visible band at 689 nm are decreased in intensity, while an obvious radical band appears at 593 nm. These spectral changes shown in red are quite similar to the second reduction of conjugate **7** at -0.80 V also shown in red (see Figure 6b). A comparison of the spectral change for **6**, **7**, and **4** during each reduction illustrates the similarity between conjugates **7**, cyanine **6**, and purpurinimide **4**, also suggesting that the purpurinimide and cyanine moieties in **7** are almost independent of each other during electron transfer processes.

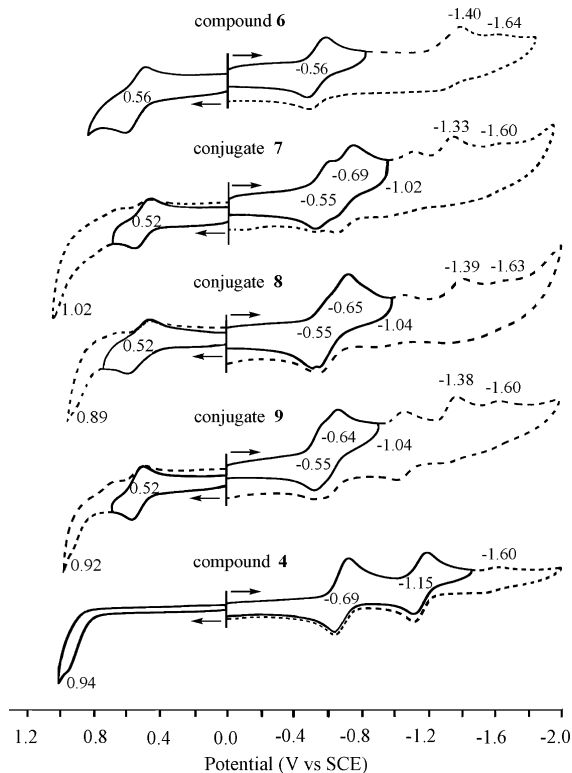


Figure 5. Cyclic voltammograms of compounds **4** and **6–9** in DMSO containing 0.1 M TBAP at a scan rate of 0.1 V/s.

Figure 7a shows the spectral changes which occur upon the one-electron oxidation of cyanine **6** at an applied potential of 0.70 V. A new absorption maximum appears at 650 nm, which is assigned as due to the cyanine radical cation. The absorption band due to the cyanine radical cation in conjugate **7** is slightly blue-shifted to 637 nm (Figure 7b). The purpurinimide radical cation could not be observed by spectroelectrochemistry because of irreversible oxidation, as shown in Figure 7c, where the absorption band due to **4** only disappears at an applied potential of 1.0 V vs SCE. The absence of an absorption band at 533 nm due to the radical anion of cyanine (Figure 6b) or the absorption band at 637 nm due to the radical cation of the cyanine (Figure 7b) confirms that there is no electron transfer from the purpurinimide moiety to the singlet excited state of the cyanine moiety or from the singlet excited state of the cyanine moiety to the purpurinimide moiety in the conjugate.

2.5. Biological Studies. 2.5.1. In Vitro PDT Efficacy.

Because of the insoluble nature of conjugates **7–9**, various formulations were used to dissolve the compounds in appropriate concentrations. Among all the formulations, reasonable solubility was obtained in both 1% Tween 80 in 5% dextrose–water solution.²² The *in vitro* PDT efficacy of conjugates **7–9** was determined in Colon26 cells by following the standard MTT assay²³ (for details, see the Experimental Procedures). In brief, the cells were incubated for 24 h with **7**, **8**, and **9** at variable concentrations and then exposed to laser light (1.0 J/cm²) at 695, 713, and 710 nm (the longest absorption wavelengths corresponding to the purpurinimide portion for the respective conjugates). The PDT efficacy (cell

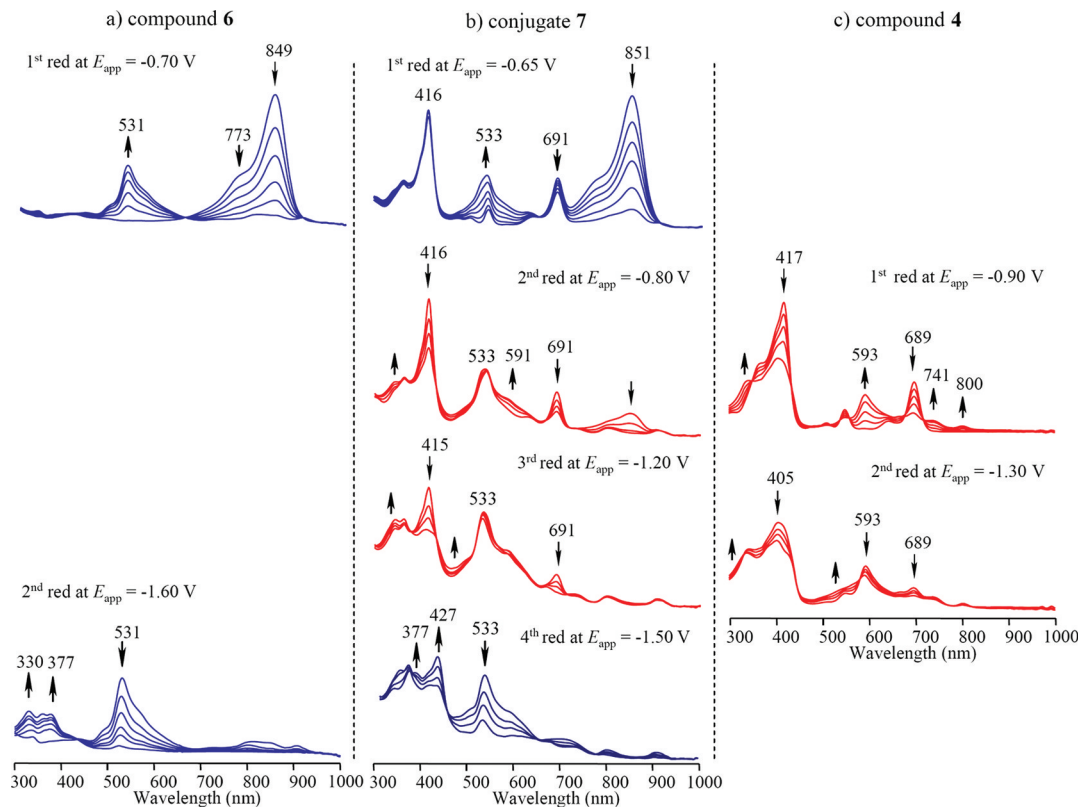


Figure 6. Thin-layer UV–visible spectra of (a) **6**, (b) **7**, and (c) **4** upon the controlled reducing potentials in DMSO containing 0.1 M TBAP. The blue spectral changes in conjugate **7** correspond to a reduction on the cyanine dye moiety. The red spectral changes are assigned at the reduction at the purpurinimide unit of the conjugate.

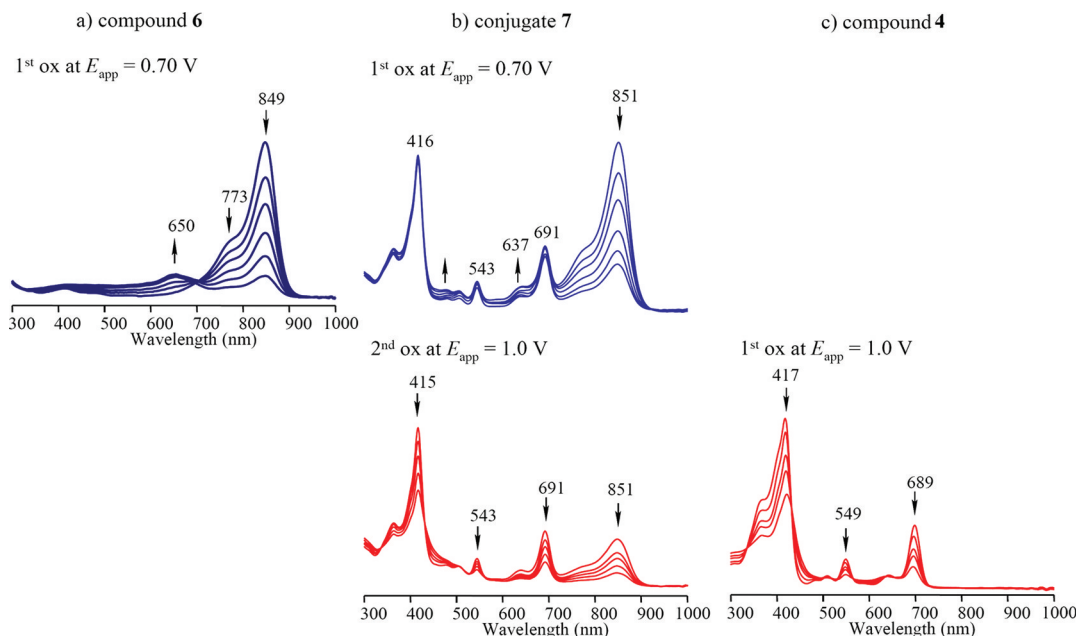


Figure 7. Thin-layer UV-visible spectra of (a) 6, (b) 7, and (c) 3 upon the controlled reducing potentials in DMSO containing 0.1 M TBAP.

kill) was calculated from 4 replicate wells in 3 separate experiments, and each standard error is representative of 3 separate experiments. The results, summarized in Figure 8 and

data. The IC_{50} values confirmed a decreased *in vitro* PDT efficacy in this series of conjugates by increasing the linker length between the purpurinimide and the cyanine dye.

2.5.2. In Vivo Fluorescence Imaging. Cyanine dye 6 has the required photophysical properties (long wavelength absorption with significant Stokes shift), for fluorescence imaging but was not tumor-avid.²⁴ To investigate the use of tumor-avid purpurinimides as vehicles to deliver the nontumor-avid cyanine dye to the tumor, we used fluorescence imaging as a tool to investigate the effect of the linker *in vivo*.²⁵ Compared to the therapeutic dose, the imaging dose was quite low, and therefore, we were able to evaluate the imaging potential of the three conjugates 7–9. Each conjugate was injected i.v. via the tail vein at a dose of 0.03 μ mol/kg into BALB/c mice (9 mice/group) bearing Colon26 tumors on the shoulder.

Figure 9 represents fluorescent images of the tumors at 24, 48, and 72 h postinjection of conjugates 7, 8, and 9 (3 mice/time point) after each drug was injected. The color scale represents fluorescence intensity, where blue is the lowest intensity, and red/white is the highest. After imaging, the mice at each time point were sacrificed, and the organs were removed and imaged *ex vivo* to demonstrate the distribution and clearance rates of the conjugates. Conjugate 8 exhibited the highest fluorescent intensity in the tumors of all the compounds at 24 h and was gradually clear from the tumor by 72 h. Conjugate 9 showed a moderate but lower fluorescence intensity than compound 8, which cleared from the tumor at a much faster rate. Interestingly, conjugate 7 gave low, barely noticeable fluorescence intensity in the tumor, which could either indicate poor fluorescence quantum yield for the cyanine dye portion of this compound or low tumor selectivity.

The *ex vivo* fluorescence intensities of various organs (ear, heart, kidney, liver, lung, muscle, small intestine, spleen, stomach, and tumors) are shown in Figure 10. As expected, conjugate 9 in which the photosensitizer is joined with the cyanine dye via a PEG linker exhibited highest fluorescence (high uptake) in the liver compared to 7 and 8. The high affinity for this compound to the liver could be due to the more

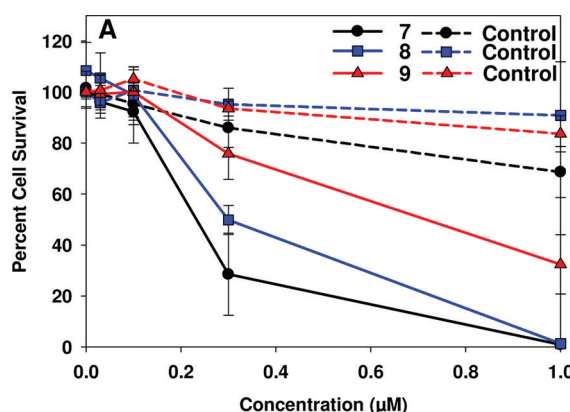


Figure 8. MTT plotted assay of 7, 8, and 9 incubated for 24 h at various concentrations with Colon26 cells followed by a light dose of 1.0 J/cm^2 at a dose rate of 3.2 mW/cm^2 .

Table 1. IC_{50} (50% Cell Kill) Concentrations of Conjugates 7, 8, and 9^a

conjugate	IC_{50} (μ M)	distance (\AA) between the two moieties
7 (short linker)	0.22	8.18
8 (medium linker)	0.32	8.55
9 (long linker)	0.69	9.85

^aAverage distance of various conformers is shown in the caption to Figure 2.

Table 1, show that increasing the distance between the photosensitizer and cyanine dye decreases the *in vitro* PDT efficacy. The LD_{50} s of the conjugates were determined by the best fit curves (plotted in SigmaPlot) to the dose-response

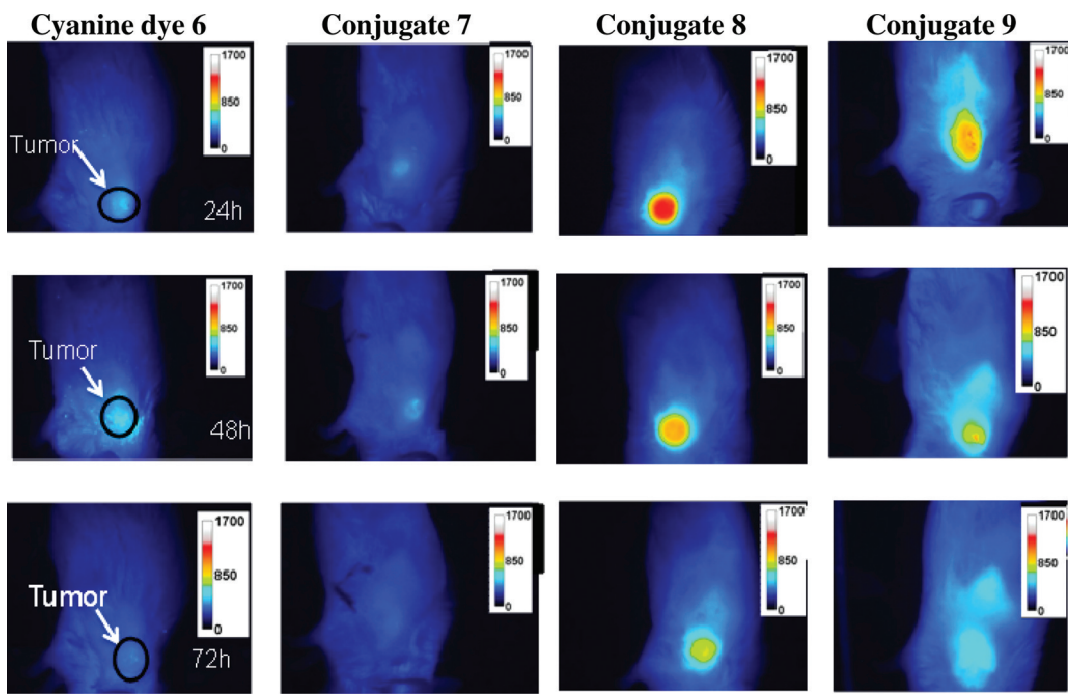


Figure 9. Comparative whole body images of conjugates 7–9 along with cyanine dye 6 (dose: $0.03 \mu\text{mol}/\text{kg}$) in BALB/c mice bearing Colon26 tumors. Images were taken at 24, 48, and 72 h postinjection using a 12 bit Nuance camera (CRI, Woburn, MA) with a 782 continuous wave laser for excitation and a 800 and 830 nm long pass filter to collect fluorescence. Images were then analyzed using Image J software.

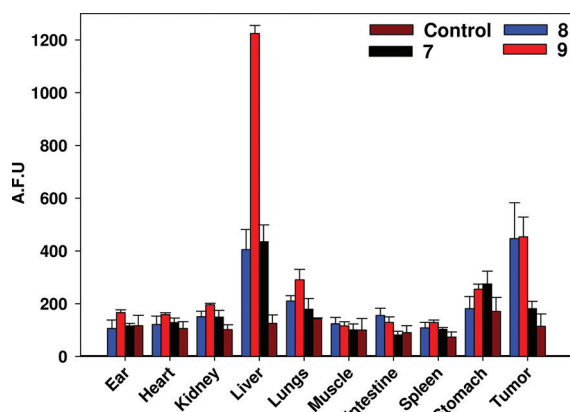


Figure 10. Fluorescence biodistribution of conjugates 7–9 and various organs [3 mice (BALB/c bearing Colon26 tumors)]. Organs from the mice were removed and then imaged/analyzed at 24 h postinjection (dose: $0.03 \mu\text{mol}/\text{kg}$). The fluorescence intensity of each organ was analyzed by Image J software.

lipophilic nature of the linker connecting the purpurinimide and cyanine dye. Interestingly, the PEG linker also showed comparable tumor avidity. Since the purpose of this study is to create a molecule that can act as both a fluorescent imaging and a therapeutic agent *in vivo*, conjugate 7 was not examined any further due to its weak uptake in tumors compared to that of the other two conjugates, determined by fluorescence imaging. However, further studies at lower time points may produce improved efficacy, and these studies with this and other agents are currently in progress.

2.5.3. Comparative *In Vivo* Tumor Uptake of the Conjugates. *In vivo* reflectance spectroscopy was used to determine the maximum uptake of the conjugates at various time points.²⁶ Mice were injected through the orbital venous plexus, the reflectance in tumors was measured at 24 and 48 h,

and the drug concentrations were determined (see Figure 11). This approach was extremely useful in providing the knowledge of the pharmacokinetic characteristics (especially the clearance from the tumor) of the conjugates and also the shift in their *in vivo* absorption. Under a similar dose of the drug ($2.5 \mu\text{mol}/\text{kg}$), conjugate 8 showed maximum tumor uptake (BALB/c mice bearing Colon26 tumors) at 24 h postinjection, which decreased over the next 24 h. Conjugate 9 showed a small increase in uptake at 48 h compared to that at 24 h.

Comparatively, conjugate 8 showed a higher tumor uptake than 9 at both 24 and 48 h. Since our objective has been to develop a candidate with both imaging and therapy capabilities and conjugate 7 showed limited PDT efficacy, it was decided not to explore its imaging potential.

2.5.4. In Vivo Photosensitizing Efficacy. Preliminary *in vivo* PDT efficacy of conjugates 8 and 9 was measured by tail vein injection into BALB/c mice (5 mice/group) bearing Colon26 tumors (average tumor volume 27 mm^3) at a dose of $2.5 \mu\text{mol}/\text{kg}$ (which gave approximately 50% tumor cure with the HPPH–cyanine dye conjugate, our lead compound).¹⁰ The tumors were illuminated with light ($135 \text{ J}/\text{cm}^2$, $74 \text{ mW}/\text{cm}^2$) at 24 h postinjection, with the best time point for the maximum photosensitizer uptake in the tumor determined by fluorescence imaging and *in vivo* reflectance spectroscopy. From the preliminary results summarized in Figure 12A, it can be seen that compared to 8, the conjugate 9 exhibited limited long-term efficacy and that all mice showed tumor regrowth at 10–12 days post-treatment. Under similar treatment parameters, conjugate 8 showed 100% tumor cure, and no tumor growth was observed at day 60. We further investigated the efficacy of conjugate 8 at variable doses (1.5, 2.0, and $2.5 \mu\text{mol}/\text{kg}$), and the light dose was kept the same ($135 \text{ J}/\text{cm}^2$, $75 \text{ mW}/\text{cm}^2$). From the results summarized in Figure 12B, it can be seen that at the lowest dose of $1.5 \mu\text{mol}/\text{kg}$, conjugate 8 showed limited efficacy, but at higher doses, a significant PDT response was

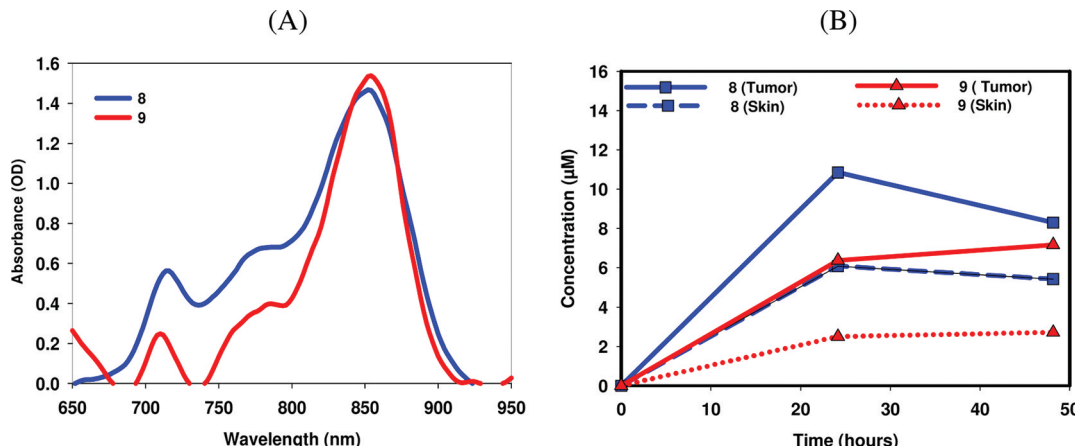


Figure 11. (A) *In vivo* absorption spectra of conjugates 7 and 8 determined by *in vivo* reflectance spectroscopy in a Colon26 tumor implanted in BALB/c mice at 24 h postinjection. (B) Tumor vs skin uptake of the conjugates at 24 and 48 h postinjection (drug dose: 2.5 $\mu\text{mol}/\text{kg}$).

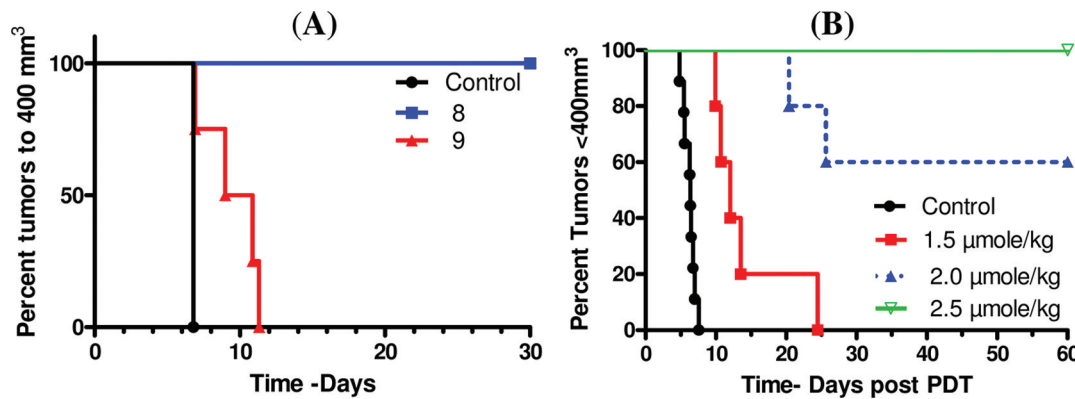


Figure 12. (A) Comparative *in vivo* photosensitizing efficacy of conjugates 8 and 9 in BALB/c mice (5 mice/group) bearing Colon26 tumors at a dose of 2.5 $\mu\text{mol}/\text{kg}$, and (B) *in vivo* efficacy of 8 at variable drug doses. The tumors were exposed to light (135 J/cm^2 and 75mW/cm²) at their longest wavelength absorption at 24 h postinjection (i.v.) of the photosensitizers. The tumor growth was measured daily. Under the treatment parameters used, the mice treated with conjugate 8 at a dose of 2.5 $\mu\text{mol}/\text{kg}$ did not show any tumor regrowth, and the tumors were flat on day 60 post-treatment.

observed (2.0 $\mu\text{mol}/\text{kg}$, 3/5 mice, and at 2.5 $\mu\text{mol}/\text{kg}$, 5/5 mice, were tumor free on day 60).

3. CONCLUSIONS

An efficient synthetic pathway was developed to create purpurinimide–cyanine dye dual functional agents. *In vitro* results suggested that increasing the carbon chain length from a short linker to a long linker decreases the PDT efficacy of the compounds. Fluorescence imaging showed that 7 (short linker) had poor imaging capabilities compared to that of 8 (medium linker) and 9 (long linker) and was not studied further. Conjugate 9 exhibited the highest liver fluorescent values. This may be due to the more lipophilic nature of the linker connecting the two molecules, which shows higher affinity to the liver. *In vivo* reflectance spectroscopy showed that conjugate 8 exhibited higher tumor uptake than 9 and should therefore produce *in vivo* PDT efficacy. The comparative *in vivo* PDT confirmed the higher efficacy of conjugate 8 over 9 and produced 100% tumor response (5/5 BALB/c mice bearing Colon26 tumors were tumor free after day 60 post-treatment), whereas 9, under similar treatment parameters showed limited PDT activity. This study with a small number of conjugates indicates that conjugate 8 with a medium length of linker shows potential for both tumor imaging and therapy. However, further

studies with a larger group of compounds should help in selecting the best candidates, and the synthesis of the related analogues is underway. The low PDT and imaging capabilities of conjugate 7 could be due to its faster *in vivo* clearance. Therefore, further studies with conjugate 7 at shorter time intervals between the injection of the drug and light treatment are also in progress.

4. EXPERIMENTAL PROCEDURES

All chemicals were of reagent grade and used as such. All reagents were purchased from Aldrich chemical company and were used as received. All photophysical experiments were carried out using spectroscopic grade solvents. Solvents were dried using standard methods unless stated otherwise. Reactions were carried out under nitrogen atmosphere and were monitored by precoated (0.20 cm) silica TLC plastic sheet (20 cm × 20 cm) strips (POLYGRAM SIL N-HR) and or/UV-visible spectroscopy. UV-visible spectra were recorded on a Varian Cary 50 Bio UV-visible spectrophotometer using dichloromethane/methanol as solvent unless otherwise specified. ¹H NMR spectra were recorded on Varian 400 spectrometers at 303 K in CDCl₃ or ~10% of CD₃OD in CDCl₃ or DMSO-d₆. Proton chemical shifts (δ) are reported in parts per million (ppm) relative to CDCl₃ (7.26 ppm), CD₃OD

(3.34 ppm) or TMS (0.00 ppm). Coupling constants (*J*) are reported in Hertz (Hz), and s, d, t, q, p, m, and br refer to singlet, doublet, triplet, quartet, pentet, multiplet, and broad, respectively. Mass spectral data (Electro Spray Ionization, ESI, by fusion) were obtained from Biopolymer Facility, Roswell Park Cancer Institute, Buffalo, NY, and HRMS data were obtained from the Mass Spectrometry Facility, Michigan State University, East Lansing, MI. Elemental analysis were done at Midwest Microlab LLC., Indianapolis, IN.

4.1. N-Amino Purpurinimide Methyl Ester (3).

Mesopurpurin-18 methyl ester (**2**) (0.138 mmol, 80 mg) was dissolved in 15 mL of anhydrous pyridine and stirred under argon. Hydrazine anhydrate (1.3 mmol, 42 mg, 42 μ L) was added to 2 mL of anhydrous pyridine, which was then added slowly to the stirring mixture. The completion of the reaction was checked by UV-vis in regular intervals until the wavelength intensity at λ_{max} of 701 nm was maximal. After 4 h, 1 N HCl (25 mL) and dichloromethane (20 mL) were added, and the stirring was continued for another 1.5 h. The reaction mixture was then transferred into a separation funnel. Additional dichloromethane (200 mL) was added, the organic layer was washed with water (200 mL \times 3). The dichloromethane (DCM) layer was separated, dried over anhydrous sodium sulfate, and filtered. The crude reaction product obtained after evaporating DCM was purified on an alumina column by eluting with a 1% MeOH/DCM solvent system to afford a purple/magenta crystal of **3²¹** (42.4 mg, 50% yield). UV-vis λ_{max} (in CH₂Cl₂): 359 nm ($\epsilon = 5.8 \times 10^4$), 416 ($\epsilon = 10.0 \times 10^5$), 548 ($\epsilon = 1.9 \times 10^5$), 643 ($\epsilon = 8.60 \times 10^3$), 700 ($\epsilon = 4.94 \times 10^4$). ¹H NMR (400 MHz, 3 mg/1 mL CDCl₃, δ ppm) 9.07, 8.95, and 8.42 (each s, 1H for SH, 10H and 20H), 5.72 (broad s, N-NH₂), 5.29 (m, 1H, for 17H), 4.33 (m, 1H for 18H), 3.63 (q, 2H for 8¹CH₂) 3.62 (s, 3H for 12CH₃), 3.61 (s, 3H for 17²CO₂CH₃), 3.33 (m, 2H for 3¹CH₂) 3.18 (s, 3H for 2CH₃), 3.00 (s, 3H for 7CH₃), 2.78 and 1.978 (m, 2H for 17¹CH₂), 2.46 (m, 2H for 17²CH₂) 1.76 (d *J* = 7.2 Hz, 3H for 18CH₃), 1.66 (t, *J* = 7.2 Hz, 3H for 8²CH₃), 1.50 (m, 3H for 3²CH₃). EIMS (*m/z*): 595 (M + H). Elemental Anal. Calcd. for C₃₄H₃₈N₆O₄: C, 68.67; H, 6.44; N, 14.13. Found: C, 68.70; H, 6.43; N, 14.01.

4.2. N-Boc Diethlyene Purpurinimide Methyl ester (4a).

Purpurin-18 methyl ester (50 mg, 0.0865 mmol) (**1**) was added to a dry 100 mL round bottomed flask and put under house vacuum for 20 min. N-Boc ethylenediamine (48.50 mg, 0.30275 mmol) was placed under nitrogen for 10 min and then added to the flask containing Purpurin-18 using a long needle. Under a nitrogen atmosphere, 5–10 mL of anhydrous DCM was added to the reaction mixture, which was stirred for 39 h, monitoring with UV-vis. A wavelength of 665 nm indicated the opening of the six-membered anhydride ring system. It was then treated with diazomethane, the intermediate amide, as methyl ester was not isolated, and immediately treated with a catalytic amount of KOH/MeOH. The base catalyzed intramolecular cyclization afforded the desired analogue exhibiting the long wavelength absorption at 707 nm. The reaction mixture was purified by preparative plates using a 5% MeOH/DCM solvent system, and the desired band was scratched off and resuspended in 5% methanol/dichloromethane. The silica was removed by filtration. Solvents were evaporated, and the residue **4a** was precipitated with DCM/n-hexane (60 mg, 86% yield). UV-vis λ_{max} (in CH₂Cl₂): 365 nm, 418 nm, 550 nm, 707 nm. ¹H NMR (400 MHz, 3 mg/1 mL CDCl₃, δ ppm) 9.40, 9.20, and 8.56 (each s, 1H for SH, 10H and 20H); 7.83 (dd, *J* =

11.6, 5.2 Hz 1H, 3¹CH=CH₂); 6.24 (d, *J* = 16.4 Hz, 1H, trans 3²CH=CH₂), 6.12, (d, *J* = 8.4 Hz, 1H cis 3²CH=CH₂); 5.46 (br s, 1H, N-H-CH₂-CH₂-N-Boc); 5.37 (d, *J* = 4 Hz, 1H for 17H), 4.62 (m, 2H, NH-CH₂-CH₂-N-Boc); 4.37 (q, 1H for 18H); 3.59 (s, 3H, 17²CO₂CH₃); 3.49 (q, 2H for NH-CH₂-CH₂-N-Boc); 3.79 (d, *J* = 5.2 Hz, 1H for 8¹CH₂); 3.73 (s, 3H for 12CH₃); 3.33 (s, 3H for 2CH₃); 3.04 (s, 3H for 7CH₃); 2.72, 2.46, 2.44, and 2.06 (each m, 1H for 2 \times 17¹H and 2 \times 17²H); 1.79 (d, *J* = 8 Hz, 3H for 18¹CH₃); 1.60 (t, *J* = 7.6 Hz 3H for 8²CH₃); -0.128 and -0.215 (br s, 1H for 2NH). EIMS (*m/z*): 721 (M + H).

4.3. Diethlyene Amino Purpurinimide Methyl Ester (4).

N-Boc diethlyene purpurinimide methyl ester (**4a**) was treated with a 4:1 ratio of TFA/dry DCM and stirred for 2 h. The TFA was removed by high vacuum for 5 h, and the remainder was purified on an alumina column with 5% MeOH/DCM as the solvent system. The resulting compound was isolated as a dark purple liquid, compound **4**, which was concentrated by evaporating the liquid under vacuum to afford dark purple crystals (54 mg, 89% yield) UV-vis λ_{max} (in CH₂Cl₂): 365 nm ($\epsilon = 4.5 \times 10^4$), 419 nm ($\epsilon = 1.18 \times 10^5$), 551 nm ($\epsilon = 4.6 \times 10^4$), 706 nm ($\epsilon = 4.2 \times 10^4$). ¹H NMR (400 MHz, 3 mg/1 mL CDCl₃, δ ppm) 9.65, 9.44, 8.78 (each s, 1H for 5H, 10H and 20H); 8.03 (dd, *J* = 17.6, 11.6 Hz, 1H, 3¹CH=CH₂), 6.45 (d, *J* = 18.0, 1H, trans 3²CH=CH₂), 6.34 (d, *J* = 11.6, 1H cis 3²CH=CH₂), 5.58 (d, *J* = 8.4 Hz, 1H for 17H); 4.81 (t, *J* = 6.8 Hz, 2H for N-CH₂-CH₂-N), 4.58 (q, *J* = 7.2 Hz, 1H for 18H), 3.95 (s, 3H, 12CH₃), 3.81 (s, 3H, 17²CO₂CH₃), 3.80 (q, *J* = 7.6 Hz, 2H, 8¹CH₂), 3.54–3.59 (m, 5H, 2CH₃ and N-CH₂-CH₂-N), 3.27 (s, 3H, 7CH₃), 2.96, 2.67, 2.62, and 2.22 (each m, 1H, 2 \times 17¹H and 2 \times 17²H), 2.00 (d, *J* = 7.2 Hz, 3H, 18CH₃), 1.82 (t, *J* = 7.6 Hz, 3H, 8²CH₃) 0.08 and 0.00 (each br s, 1H, 2NH). EIMS (*m/z*): 621.1 (M + H). Elemental Anal. Calcd. for C₄₀H₄₈N₆O₆: C, 69.66; H, 6.50; N, 13.54. Found: C, 68.63; H, 6.51; N, 12.88.

4.4. N-Boc Glycol Purpurinimide Methyl Ester (5a).

N-Boc-2,2'-(ethylene-1,2-dioxy) bisethylamine was prepared by following the literature procedure.¹⁰ It (50 mg, 0.2015 mmol) was dissolved in 5 mL of dry DCM. This was added to a stirring mixture of purpurin-18 methyl ester (50 mg, 0.0865 mmol) in 10 mL of dry DCM. The reaction was stirred for 39 h under a nitrogen atmosphere with UV-vis monitoring (a shift from 700 nm to 665 nm). The reaction was then treated with diazomethane/KOH/MeOH until a red shift to 707 nm indicated the reaction was complete. A preparation scale TLC separation was done with a 5% MeOH/DCM solvent system, and the desired band was scratched off, and the desired product was isolated by following the method as discussed above to yield compound **5a** (60 mg, 86% yield). UV-vis λ_{max} (in CH₂Cl₂): 365.1 nm, 419 nm, 549 nm, 707 nm. ¹H NMR (400 MHz, 3 mg/1 mL CDCl₃, δ ppm) 9.58, 9.32, and 8.56 (each s, 1H for 5H, 10H and 20H), 7.88 (dd, *J* = 8.0, 10.4 Hz 1H, 3¹CH=CH₂); 6.24 (d, *J* = 16.0 Hz, 1H, trans 3²CH=CH₂); 6.14 (d, *J* = 11.6, 1H cis 3²CH=CH₂); 5.32 (m, 1H for 17H); 5.10 (br s, 1H for N-CH₂-CH₂-(O-CH₂)₂-NHBOC); 4.73 (t, *J* = 8.0 Hz, 2H for N-CH₂-CH₂-(O-CH₂)₂-NHBOC); 4.34 (q, 1H for 18H); 2.70, 2.40, 2.35, and 1.98 (each m 1H, 2 \times 17¹H and 2 \times 17²H); -0.05 and -0.15 (br s, 1H for 2NH). EIMS (*m/z*): 809 (M + H).

4.5. N-Glycol Purpurinimide Methyl Ester (5). Purpurin-18-N-Boc-glycol-imide (**5a**) was treated with a 4:1 ratio of TFA/Dry DCM and stirred for 2 h. The reaction was concentrated by evaporating under vacuum. The crude mixture

was purified on an alumina column with 5% MeOH/DCM as the solvent system. The resultant compound after the standard workup afforded dark purple crystals of **5** (54 mg, 89% yield). UV-vis λ_{max} (in CH_2Cl_2): 365 nm ($\epsilon = 4.5 \times 10^4$), 419 nm ($\epsilon = 1.18 \times 10^5$), 551 nm ($\epsilon = 2.1 \times 10^5$), 707 nm ($\epsilon = 4.30 \times 10^4$). ^1H NMR (400 MHz, 3 mg/1 mL CDCl_3 , δ ppm) 9.58, 9.34, and 8.56 (each s, 1H for 5H, 10H and 20H); 7.90 (dd, $J = 11.6, 11.6$ Hz, 1H for $3^1\text{CH}=\text{CH}_2$); 6.30 (d, $J = 16.4$ Hz, 1H for *trans*- $3^2\text{CH}=\text{CH}_2$); 6.15 (d, $J = 10.4$ Hz, 1H for *trans*- $3^2\text{CH}=\text{CH}_2$); 5.33 (m, 1H for 17H); 4.73 (t, $J = 1.6$ Hz, 2H for $\text{N}-\text{CH}_2-\text{CH}_2-(\text{O}-\text{CH}_2)_2-\text{NH}_2$); 4.63 (q, 1H for 18H); 4.07 (m, 2H for $\text{N}-\text{CH}_2-\text{CH}_2-(\text{O}-\text{CH}_2)_2-\text{NH}_2$); 3.85 (m, 2H for $\text{N}-(\text{O}-\text{CH}_2)_2-\text{CH}_2-\text{CH}_2-\text{NH}_2$); 3.79 (s, 3H for 12CH₃); 3.70 (t, $J = 36$ Hz, $\text{N}-(\text{CH}_2)_2-\text{O}-\text{CH}_2-\text{CH}_2-\text{O}-(\text{CH}_2)_2\text{NH}_2$); 3.62 (q, 2H for 8^1CH_2); 3.56 (s, 3H for $17^2\text{CO}_2\text{CH}_3$); 3.51 (m, 2H for $\text{N}-(\text{CH}_2)_2-\text{O}-\text{CH}_2-\text{CH}_2-\text{O}-(\text{CH}_2)_2\text{NH}_2$); 3.34 (s, 3H for 18 CH₃); 3.14 (s, 3H for 7CH₃); 2.80, 2.70, 2.40, and 1.99 (each m 1H, 2 \times 17^1H and 2 \times 17^2H); 1.95 (m, 2H for $\text{N}-(\text{O}-\text{CH}_2)_2-\text{CH}_2-\text{CH}_2-\text{NH}_2$); 1.86 (broad s, 2H for NH₂); 1.74 (d, $J = 7.2$ Hz, 3H for 18CH₃); 1.65 (t, $J = 7.6$ Hz, 3H for 8^2CH_3); 0.059 and -0.146 (broad s, 1H for 2NH). EIMS (m/z): 709 (M + H). Elemental Anal. Calcd. for $\text{C}_{40}\text{H}_{48}\text{N}_6\text{O}_6$: C, 67.78; H, 6.83; N, 11.86. Found: C, 67.59; H, 6.60; N, 10.90.

4.6. Cyanine Dye (6). To a dry round bottomed flask containing IR-820 (342 mg, 0.402 mmol) stirring in anhydrous DMF was added 4-carboxythiophenol (186.2 mg, 1.20 mmol), and the mixture was stirred overnight under a nitrogen atmosphere. The crude reaction product obtained after the standard workup was purified over a silica column using a 5–25% DCM/MeOH solvent system, and a green liquid was collected. The liquid was concentrated by evaporation under vacuum and scratched to afford dark green crystals of **6** yield (270 mg, 80%). UV-vis λ_{max} (in MeOH) 835 nm ($\epsilon = 1.96 \times 10^5$); ^1H NMR (400 MHz, 3 mg/1 mL MeOH, δ ppm) 8.87 (d, 2H, $J = 14$ Hz), 8.15 (d, 2H, $J = 14$ Hz), 8.79–7.99 (m, 6H), 7.57–7.63 (m, 4H), 7.44 (t, 2H, $J = 7.2$ Hz), 7.36 (d, 2H, $J = 8.4$ Hz), 6.40 (d, 2H, $J = 14$ Hz), 4.27 (t, 4H, $J = 7.6$ Hz), 2.85–2.92 (m, 8H), 1.93–2.10 (m, 10 H), 1.77 (s, 12H). EIMS (m/z): 989.4 (M⁺ + 2Na). HRMS: Calcd. for $\text{C}_{53}\text{H}_{56}\text{N}_2\text{O}_8\text{S}_3\text{Na}$: 967.3097. Found: 967.3127.

4.7. Conjugate 7. In a dry round bottomed flask containing cyanine dye **6** (121.62 mg, 0.1289 mmol), DMTMM (39.25 mg, 1.1 equiv) was stirred in 5 mL of anhydrous DMF under a nitrogen atmosphere for 2 h. *N*-Amino purpurinimide methyl ester **3** (80 mg, 0.1289 mg) was stirred in 5 mL of anhydrous DMF in a separate round bottomed flask and was added to the flask containing the cyanine dye after 2 h. The reaction was stirred overnight and was purified by a preparative silica TLC plate using a 20% MeOH/DCM solvent system. The desired band was collected and resuspended in 5% methanol dichloromethane. It was then filtered, and the solvents were concentrated. The residue was crystallized/precipitated as dark purple crystals; yield (40 mg, 32%). UV-vis λ_{max} (in MeOH): 361 nm ($\epsilon = 3.9 \times 10^4$), 412 ($\epsilon = 9.6 \times 10^4$), 544 ($\epsilon = 1.7 \times 10^4$), 693 ($\epsilon = 4.5 \times 10^4$), 837 ($\epsilon = 1.5 \times 10^5$). ^1H NMR (400 MHz, 3 mg/1 mL MeOH, δ ppm) 9.72, 9.37, 8.81 (each s, 1H, for 5H, 10H and 20H); 8.78 (d, $J = 2.4$ Hz, 2H, cyanine dye F); 8.29 (d, $J = 8$ Hz, 2H, cyanine dye B); 8.09 (m, 6H, cyanine dye H and D); 7.81 (d, $J = 8.8$ Hz, 2H, cyanine dye G); 7.64 (t, $J = 12$ Hz, 4H, cyanine dye C); 7.51 (t, $J = 8$ Hz, 2H, cyanine dye A); 6.50 (d, $J = 16$ Hz, 3H, cyanine dye E); 5.01 (m, 2H cyanine dye SO₃H), 4.91 (m, 1H for 17H); 4.35 (m, 4H for cyanine dye H and 1H for

18H); 3.80(br doublet, 4H, 2H for 3^1CH_2 and 2H for 8^1CH_2); 3.75 (d, 7H, 4H for $17^2\text{CO}_2\text{CH}_3$ and 3H); 3.35 (H_2O peak and hidden 3H for 12CH₃ singlet peak); 3.335 and 3.225 (s, 4H, 3 for 7CH₃ and 1H); 2.90 (m, 5H for cyanine dye K and L); 2.50 (m, 2H, 17^2CH_3 within DMSO peak); 2.32 (m, 2H for 17^1CH_2); 2.06–1.52 (many multiplets, 41H, 12H for cyanine dye J and N, 3H for cyanine dye M, 9H for 3^2CH_3 , 18^1CH_3 and 8^2CH_3 , and 17 H). EIMS (m/z): 1520 (M – H). HRMS: Calcd. for $\text{C}_{87}\text{H}_{92}\text{N}_8\text{O}_{11}\text{S}_3$: 1520.6048. Found: 1520.6048.

4.8. Conjugate 8. In a dry round bottomed flask, cyanine dye **6** (92.4 mg, 0.098 mmol) and DMTMM (30 mg, 0.1078 mmol) were stirred in 5 mL of anhydrous DMF in a nitrogen atmosphere for 2 h. Diethyllyeaminopurpurinimide methyl ester **4** (70 mg, 0.098 mmol) was stirred in 5 mL of anhydrous DMF in a separate round bottomed flask and was added into the flask containing the cyanine dye after 2 h. The reaction was stirred overnight and was purified on a preparation scale TLC plate using a 20% MeOH/DCM solvent system. The desired fraction was collected, and the residue obtained after evaporating the solvent was crystallized/precipitated with DCM/hexane as dark purple crystals; yield (35 mg, 37%). UV-vis λ_{max} (in MeOH): 365 nm ($\epsilon = 3.8 \times 10^4$), 418 nm ($\epsilon = 8.2 \times 10^4$), 549 nm ($\epsilon = 1.6 \times 10^4$), 707 nm ($\epsilon = 4.6 \times 10^4$), 842 nm ($\epsilon = 1.6 \times 10^5$). ^1H NMR (400 MHz, 3 mg/1 mL MeOH, δ 9.59, 9.42, and 8.86 (each s, 1H for 5H, 10H and 20H); 8.61 (d, 2H for cyanine dye f, $J = 14$ Hz); 8.16 (dd, $J = 8$ Hz, 40 Hz, 1H, $3^1\text{CH}=\text{CH}_2$); 8.06 (d, 2H for cyanine dye B, $J = 8.4$ Hz); 7.98–7.95 (m, 4H for cyanine dye H and D); 7.73–7.67 (m, 4H for cyanine dye G and C); 7.47 (t, 2H for cyanine dye A, $J = 7.2$ Hz); 7.34 (d, 2H for cyanine dye E, $J = 8.4$ Hz); 6.38 (t, 3H, 2H for cyanine dye E, 1H for *trans*- $3^2\text{CH}=\text{CH}_2$, $J = 14$ Hz); 6.20 (d, 1H for *cis*- $3^2\text{CH}=\text{CH}_2$, $J = 11.6$); 5.12 (d, 1H for 17H, $J = 1.2$ Hz); 4.53–4.40 (m, 3H, 1H for 18H and 2H for $\text{N}-\text{CH}_2-\text{CH}_2-\text{N}$); 4.24 (broad s, 3H for cyanine dye I); 3.81 (s, 3H for 12CH₃); 3.69 (m, 1H for NH); 3.60 (s, 3H for $17^2\text{CO}_2\text{CH}_3$); 3.39–3.31 (m, 2H for 8^1CH_2 , 3H for 2CH₃ and 2H for $\text{N}-\text{CH}_2-\text{CH}_2-\text{N}$, 8H for cyanine dye K and L); 3.13 (s, 3H for 7CH₃); 2.33–2.20 (each m, 1H for, 2 \times 17^1H and 2 \times 17^2H); 2.10–2.08 (each m, 8H for cyanine dye J and N); 1.925 (m, 3H for 18CH₃); 1.74–1.52 (m, 15H, 3H for 8^2CH_3 and 12H for cyanine dye M); -0.35 and -0.41 (each br s, 1H for 2NH). EIMS (m/z): 1546 (M – H). HRMS Calcd. for $\text{C}_{89}\text{H}_{94}\text{N}_8\text{O}_{11}\text{S}_3$: 1546.6204. Found: 1546.6244.

4.9. Conjugate 9. In a dry round bottomed flask, cyanine dye **6** (142.7 mg, 0.151 mmol) and DMTMM (45.96 mg, 0.1661 mmol) were stirred in 5 mL of anhydrous DMF in a nitrogen atmosphere for 2 h. *N*-Glycolpurpurinimide methyl ester **5** (90 mg, 0.151 mmol) stirred in 5 mL of anhydrous DMF in a separate round bottomed flask was added to the flask containing the cyanine dye after 2 h. The reaction was stirred overnight and was purified on a preparation scale TLC plate using a 20% MeOH/DCM solvent system as discussed for the foregoing compound. The desired fraction was collected and concentrated, crystallized with DCM/hexane to afford dark purple crystals; yield (40 mg, 32%). UV-vis λ_{max} (in MeOH): 366 nm ($\epsilon = 4.5 \times 10^4$), 416 nm ($\epsilon = 1.0 \times 10^5$), 549 nm ($\epsilon = 2.7 \times 10^4$), 707 nm ($\epsilon = 5.8 \times 10^4$), 842 nm ($\epsilon = 2.1 \times 10^5$). ^1H NMR (400 MHz, 3 mg/1 mL MeOH): δ 9.67, 9.46 and 8.88 (each s, 1H for 5H, 10H and 20H); 8.62 (d, 2H for cyanine dye f, $J = 14$ Hz); 8.10 (d, 4H, cyanine dye j, $J = 11.6$ Hz); 7.85 (m, 4H, cyanine dye M); 7.79 (d, 2H for cyanine dye a, $J = 7.2$ Hz); 7.40 (d, 2H for cyanine dye b, $J = 7.2$ Hz); 6.39 (m, 3H, 1H for $3^1\text{CH}=\text{CH}_2$ and 2H for cyanine dye e); 6.19 (d, 1H

for $3^2\text{CH}=\text{CH}_2$, $J = 7.6$ Hz); 5.18 (m, 1H for *cis*- $3^2\text{CH}=\text{CH}_2$); 4.4 (m, 1H for 18H); 4.2 (m, 1H for 17H); 3.75 (s, 3H for 12 CH₃); 3.51 (s, 3H for 2 CH₃); 3.30 (s, 3H for $17^2\text{CO}_2\text{CH}_3$); 3.15 (s, 3H for 7 CH₃); 2.80 (m, 8H for cyanine dye i and j); 2.60, 2.55, 2.40, and 2.36 (each m, 1H for, 2 \times 17¹H and 2 \times 17²H); 1.90 (m, 5H for cyanine dye c and h); 1.63 (s, 3H for 18 CH₃); 1.50 (t, 3H for 8^2CH_3 , $J=7.2$ Hz); -0.35 and -0.41 (each br s, 1H for 2NH). EIMS (*m/z*): 1634 (M - H); HRMS Calcd. for C₉₃H₁₀₃N₈O₁₃S₃: 1634.6746. Found: 1634.6729.

4.10. In Vivo Fluorescence Imaging. Fluorescence imaging was performed using approved protocols in accordance with the Guide for the Use of Laboratory Animals. A 12 bit Nuance camera (CRI, Woburn, MA) was used to image the conjugates *in vivo* using a 782 continuous wave laser for an excitation source. The fluorescence was collected after filtering through two 600 nm long pass filters in series and 800 and 830 nm long pass filters. Prior to imaging, BALB/c mice bearing Colon26 tumors on the shoulder with an average diameter of 4–5 mm were shaved and depilated with Nair cream to remove the hair over the tumor and the surrounding skin. Conjugates 7, 8, and 9 were injected via the tail vein at 0.03 $\mu\text{mol}/\text{kg}$. At 24, 48, and 72 h postinjection, mice were anesthetized with ketamine/xylene (100/10 mg/kg), placed in the light box, and imaged. The localization and biodistribution of the conjugates were determined by sacrificing 3 mice/time points and imaging the organs. The images were processed using an image calculator.²⁷

4.11. In Vivo Photosensitizing Efficacy. BALB/c mice (5 mice/group) were implanted subcutaneously in the right shoulder with 1×10^6 Colon26 cells per 50 μL of RPMI-1640 medium. When tumors grew to 4–5 mm diameter, mice were injected with 2.5 $\mu\text{mol}/\text{kg}$ of 8 and 9 via tail vein injection. Twenty-four hours postinjection, the mice were restrained within Plexiglas holders, and exposed tumors were treated with laser light for 135 J/cm² at 75mW/cm². Following treatment, tumor growth was monitored daily and measured with calipers along the length and width of the tumors. Tumor volumes were calculated by using the formula $V = LXW^2/2$. Mice were considered cured if no palpable tumor grew within 30 days of being treated, or they were euthanized when the tumor volume reached 400 mm³.

4.12. Molecular Modeling. **4.12.1. Conjugate Structures.** The three-dimensional structures of purpurinimide-cyanine dye conjugates (7–9) were built with SYBYL molecular modeling software, version 8.0 (Tripos Inc., St. Louis, MO). The purpurinimide moiety was taken from previous studies²⁸ utilizing appropriate crystal structure. The cyanine dye moiety was built from a SYBYL fragment library and standard geometry using the extended conformation. Both moieties were fully energy optimized with a semiempirical molecular orbital method, PM3, using the Spartan 02 software (Wave function Inc., Irvine, CA). Finally, energy optimized moieties were joined with specific linkers with standard geometry using SYBYL software. Each conjugate as a whole was again energy optimized with PM3 using Spartan software.

4.12.2. Conjugate Conformations. The PM3 energy optimized structure for each conjugate was used as the initial conformation for limited conformational search to explore the conformational flexibility of these conjugates. Because of the size of molecules, molecular mechanics instead of the molecular orbital method was used for this study. The stochastic conformational search was performed using Molecular

Operating Environment (MOE) software, version 2010.10, from Chemical Computing Group (Montreal, Quebec, Canada). Standard MMFFs force field and charges were used for the stochastic conformational search where the dihedral angles were randomly modified, followed by energy minimization in dihedral angles first, then energy minimization in Cartesian space. During the conformational search, the chiral centers were maintained as the original structure. No attempt was made to perform an exhaustive conformational search due to uncertainty in the environment of the conjugate in the cell or in an *in vivo* situation.

4.13. Photophysical Properties. Femtosecond transient absorption spectroscopy experiments were conducted using an ultrafast source, Integra-C (Quantronix Corp.), an optical parametric amplifier, TOPAS (Light Conversion Ltd.), and a commercially available optical detection system, Helios, provided by Ultrafast Systems, LLC. The source for the pump and probe pulses were derived from the fundamental output of Integra-C (780 nm, 2 mJ/pulse and fwhm = 130 fs) at a repetition rate of 1 kHz. Seventy-five percent of the fundamental output of the laser was introduced into TOPAS, which has optical frequency mixers resulting in a tunable range from 285 to 1660 nm, while the rest of the output was used for white light generation. Prior to generating the probe continuum, a variable neutral density filter was inserted in the path in order to generate a stable continuum, then the laser pulse was fed to a delay line that provides an experimental time window of 3.2 ns with a maximum step resolution of 7 fs. In our experiments, a wavelength between 350 to 450 nm of TOPAS output, which is the fourth harmonic of signal or idler pulses, was chosen as the pump beam. As this TOPAS output consists of not only desirable wavelength but also unnecessary wavelengths, the latter were deviated using a wedge prism with a wedge angle of 18°. The desirable beam was irradiated at the sample cell with a spot size of 1 mm diameter where it was merged with the white probe pulse in a close angle (<10°). The probe beam after passing through the 2 mm sample cell was focused on a fiber optic cable, which was connected to a CCD spectrograph for recording the time-resolved spectra (410–1600 nm). Typically, 2500 excitation pulses were averaged for 5 s to obtain the transient spectrum at a set delay time. Kinetic traces at appropriate wavelengths were assembled from the time-resolved spectral data. All measurements were conducted at room temperature, 295 K.

The fluorescence measurements were carried out with an absolute PL quantum yield measurement system (Hamamatsu photonics Co., Ltd., C9920-02) with excitation at 680 nm.

4.14. Electrochemical Measurements. Cyclic voltammetry was carried out with an EG&G Model 173 potentiostat/galvanostat. A homemade three-electrode cell was used and consisted of a glassy carbon working electrode, a platinum wire counter electrode, and a saturated calomel reference electrode (SCE). The SCE was separated from the bulk of the solution by a fritted-glass bridge of low porosity which contained the solvent/supporting electrolyte mixture. All potentials are referenced to the SCE.

UV-visible spectroelectrochemical experiments were performed with an optically transparent platinum thin-layer electrode of the type described in the literature.²⁹ Potentials were applied with an EG&G Model 173 potentiostat/galvanostat. Time-resolved UV-visible spectra were recorded with a Hewlett-Packard Model 8453 diode array rapid scanning spectrophotometer.

Tetra-*n*-butylammonium perchlorate (TBAP, ≥ 99%) was recrystallized from ethyl alcohol and dried under vacuum at 40 °C for at least one week prior to use. Dimethylsulfoxide (DMSO, ≥ 99.9%) were obtained from Sigma-Aldrich Chemical Co. and used without further purification.

■ ASSOCIATED CONTENT

S Supporting Information

The NMR/Mass spectra of compounds 3–9, the HPLC profiles of conjugates 7–9, and the experimental details of MTT assay and in vivo reflectance spectroscopy. This material is available free of charge via the Internet at <http://pubs.acs.org>.

■ AUTHOR INFORMATION

Corresponding Author

*E-mail: ravindra.pandey@roswellpark.org.

■ ACKNOWLEDGMENTS

This research was supported by Grants-in-Aid (Nos. 20108010 and 23750014) and the Global COE program “Global Education and Research Center for Bio-Environmental Chemistry” of Osaka University from the Ministry of Education, Culture, Sports, Science and Technology, Japan and KOSEF/MEST through WCU project (R31-2008-000-10010-0) from Korea to S.F. and The Robert Welch Foundation (Grant E-680) to K.M.K. and CA 127369 (NIH) to R.K.P.

■ REFERENCES

- (1) Dougherty, T. J. (1996) A brief history of clinical photodynamic therapy development at Roswell Park Cancer Institute. *J. Clin. Laser Med. Surg.* 14, 219–221.
- (2) Pandey, R. K., Goswami, L. N., Chen, Y., Gryshuk, A., Missett, J. R., Oseroff, A., and Dougherty, T. J. (2006) Nature: A rich source for developing multifunctional agents. Tumor-imaging and photodynamic therapy. *Lasers Surg. Med.* 38, 445–467.
- (3) Celli, J. P., Bryan, Q., Spring, B. Q., Rizvi, I., Evans, C. L., Samkoe, K. S., Verma, S., Pogue, B. W., and Hasan, T. (2010) Imaging and photodynamic therapy: mechanisms, monitoring, and optimization. *Chem. Rev.* 110, 2795–2838.
- (4) Ethirajan, M., Saenz, C., Dobhal, M., and Pandey, R. K. (2008) The Role of Porphyrin Chemistry in Tumor Imaging and Photodynamic Therapy, in *Advances in Photodynamic Therapy* (Hamblin, M. R., and Mrocz, P., Eds.) Artech House, Boston, MA.
- (5) Ethirajan, M., Chen, Y., Joshi, P., and Pandey, R. K. (2011) The role of porphyrin chemistry in tumor imaging and photodynamic therapy. *Chem. Soc. Rev.* 40, 340–362.
- (6) Dougherty, T. J., Gomer, C. J., Henderson, B. W., Jori, G., Kessel, D., Korbelik, M., Moan, J., and Peng, Q. (1998) Photodynamic therapy. *J. Natl. Cancer Inst.* 90, 889–905.
- (7) Henderson, B. W., and Dougherty, T. J. (1992) How does photodynamic therapy work? *Photochem. Photobiol.* 55, 145–157.
- (8) Macdonald, I., and Dougherty, T. J. (2001) Basic principles of photodynamic therapy. *J. Porphyrins Phthalocyanines* 5 (105), 2001–2011.
- (9) Gryshuk, A., Chen, Y., Goswami, L. N., Pandey, S., Missett, J. R., Ohulchansky, T., Potter, W., Prasad, P. N., Oseroff, A., and Pandey, R. K. (2007) Structure-Activity relationship among purpurinimides and bacteriopurpurinimides: Trifluoromethyl substituent enhanced the photosensitizing efficacy. *J. Med. Chem.* 50, 1754–1767.
- (10) Chen, Y., Gryshuk, A., Achilefu, S., Ohulchansky, T., Potter, W., Zhong, T., Morgan, J., Chance, B., Prasad, P. N., Henderson, B. W., Oseroff, A., and Pandey, R. K. (2005) A novel approach to a bifunctional photosensitizer for tumor imaging and phototherapy. *Bioconjugate Chem.* 16, 1264–1274.
- (11) Massoud, T. F., and Gambhir, S. S. (2003) Molecular imaging in living subjects: seeing fundamental biological process in a new light. *Genes Dev.* 17, 545–580.
- (12) Brindle, K. (2008) New approaches for imaging tumor responses to treatment. *Nat. Rev. Cancer* 8, 94–107.
- (13) Pandey, R. K., James, N., Chen, Y., and Dobhal, M. P. (2008) Cyanine dye based compounds for tumor imaging with and without photodynamic therapy. *Top. Heterocycl. Chem.* 14, 41–74.
- (14) Jager, H. R., Taylor, M. N., Theodosy, T., and Hopper, C. (2005) MR imaging-guided interstitial photodynamic laser therapy for advanced head and neck tumors. *Am. J. Neuroradiol.* 26, 1193–1200.
- (15) Mishra, A., Behera, R. K., Behera, P. K., Mishra, B. K., and Behera, G. B. (2000) Cyanines during the 1990s: A review. *Chem. Rev.* 100, 1973–2012.
- (16) Ornelas, C., Lodescar, R., Durandin, A., Canary, J. W., Pennell, R., Liebes, L. F., and Weck, M. (2011) Combining aminocyanine dyes with polyamide dendrons: A promising strategy for imaging in the near-infrared Region. *Chem.—Eur. J.* 17, 3619–3629.
- (17) Narayanan, N., and Patonay, G. (1995) A new method for the synthesis of Heptamethine cyanine dyes: Synthesis of a new near-infrared fluorescent labels. *J. Org. Chem.* 60, 2391–2395.
- (18) Majumdar, S. R., Majumdar, R. B., Grant, C. M., and Waggoner, A. S. (1996) Cyanine-labeling reagents: sulfobenzindocyanine succinimidyl esters. *Bioconjugate Chem.* 7, 356–362.
- (19) Strekowsky, L., Mason, C. J., Lee, H., Gupta, R., Sowell, J., and Patonay, G. (2003) Synthesis of water-soluble near infrared cyanine dyes functionalized with 9 succiniimidoxyl-carbonyl group. *J. Heterocycl. Chem.* 40, 913–916.
- (20) Zheng, G., Potter, R. W., Camacho, S. H., Missett, J. R., Wang, G., Bellnier, D. A., Henderson, B. W., Rodgers, M. A., Dougherty, T. J., and Pandey, R. K. (2001) Synthesis, photophysical properties, tumor uptake, and preliminary in vivo photosensitizing efficacy of a homologous series of 3-(1'-Alkyloxy)ethyl-3-devinylpurpurin-18-N-alkylimides with variable lipophilicity. *J. Med. Chem.* 44, 1540–1559.
- (21) Mironov, A. F., Grin, M. A., Tsiprovs'kiy, A. G., Kachala, V. V., Karmakova, T. A., Pltyutinskaya, A. D., and Yakubovskaya, R. I. (2003) New bacteriochlorin derivatives with a fused N-aminoimide ring. *J. Porphyrins Phthalocyanines* 7, 725–730.
- (22) Pandey, S. K., Gryshuk, A. L., Sajjad, M., Zheng, X., Chen, Y., Abuzeid, M. M., Morgan, J., Charlamisinau, I., Nabi, H. A., Oseroff, A., and Pandey, R. K. (2005) Multimodality agents for tumor imaging and PDT: A possible see and treat approach. *J. Med. Chem.* 48, 6286–6295.
- (23) Kawada, K., Yonei, T., Ueoka, H., Kiura, K., Tabata, M., Takigawa, N., Harada, M., and Tanimoto, M. (2002) Comparison of chemosensitivity tests. Clonogenic assay versus MTT assay. *Acta Med. Okayama* 56 3, 129–134.
- (24) Patterson, M. S., Schwartz, E., and Wilson, B. C. (1989) Quantitative reflectance spectrophotometry for the noninvasive measurement of photosensitizer concentration in tissue during photodynamic therapy. *SPIE 1065*, 115–122.
- (25) Potter, W. R., Bellnier, D. A., Pandey, R., Parsons, J. R., and Dougherty, T. J. Sensitizer pharmacokinetics by in vivo reflection spectroscopy, unpublished results.
- (26) Zeng, G., Chen, Y., Intes, X., Chance, B., and Glickson, J. D. (2004) Contrast-enhanced near IR optical imaging for subsurface cancer detection. *J. Porphyrins Phthalocyanines* 8, 1106–1117.
- (27) <http://rsb.info.nih.gov/ij/>
- (28) Pandey, S. K., Zheng, X., Morgan, J., Missett, J. R., Liu, T. H., Shibata, M., Bellnier, D. A., Oseroff, A. R., Henderson, B. W., Dougherty, T. J., and Pandey, R. K. (2007) Purpurinimide carbohydrate conjugates: effect of the position of the carbohydrate moiety in photosensitizing efficacy. *Mol. Pharm.* 4, 448–464.
- (29) Lin, X. Q., and Kadish, K. M. (1985) Vacuum-tight thin-layer spectroelectrochemical cell with a doublet platinum gauze working electrode. *Anal. Chem.* 57, 1498–1501.